Strathprints Institutional Repository

Lücking, Charlotte and Colombo, Camilla and McInnes, Colin (2011) *A passive de-orbiting strategy for high altitude CubeSat missions using a deployable reflective balloon.* In: 8th IAA Symposium on Small Satellites, 2011-04-04 - 2011-04-08, Berlin.

A Passive De-orbiting Strategy for High Altitude CubeSat Missions using a Deployable Reflective Balloon

Charlotte Lücking, Camilla Colombo, Colin R. McInnes
Advanced Space Concepts Laboratory, University of Strathclyde
Glasgow G1 1XJ, UK, charlotte.lucking@strath.ac.uk

Abstract: A de-orbiting strategy for small satellites, in particular CubeSats, is proposed which exploits the effect of solar radiation pressure to increase the spacecraft orbit eccentricity so that the perigee falls below an altitude where atmospheric drag will cause the spacecraft orbit to naturally decay. This is achieved by fitting the spacecraft with an inflatable reflective balloon. Once this is fully deployed, the overall area-to-mass ratio of the spacecraft is increased; hence solar radiation pressure and aerodynamic drag have a greatly increased effect on the spacecraft orbit. An analytical model of the orbit evolution due to solar radiation pressure and the J_2 effect as a Hamiltonian system shows the evolution of an initially circular orbit. The maximum reachable orbit eccentricity as a function of semi-major axis and area-to-mass ratio can be found and used to determine the size of balloon required for de-orbiting from circular orbits of different altitudes. A system design of the device is performed and the feasibility of the proposed de-orbiting strategy is assessed and compared to the use of conventional thrusters. The use of solar radiation pressure to increase the orbit eccentricity enables passive de-orbiting from significantly higher altitudes than conventional drag augmentation devices.

Notation:

a	semi-major axis [km]
a_{SRP}	acceleration due to solar rad. pressure [km/s]
α	solar radiation pressure effect parameter
$n_{\odot}$	average orbital rate of the Earth around the sun [rad/s]
c	speed of light in vacuum [m/s]
c_R	coefficient of reflectivity
e	eccentricity
F_S	solar energy flux density at distance of spacecraft [W/m^2]
J_2	oblateness coefficient of the Earth
μ	gravitational parameter of the Earth [km^3/s^2]
ϕ	in-plane sun-perigee angle [rad]
R_E	average radius of the Earth [km]
σ	spacecraft area-to-mass ratio [m^2/kg]
κ	J_2 effect parameter

1. Introduction

There is a growing interest in picosatellite projects, in particular CubeSats, whose modest size and standardised launcher interface lowers costs for launch and deployment into orbit. CubeSat missions are typically restricted to Low Earth Orbits (LEO) because of de-orbiting requirements. They can be deployed at an altitude where orbit decay due to atmospheric drag can be guaranteed because they characteristically do not accommodate a propulsion system to perform orbital manoeuvres. This is due to their small size and simple design which are hard to combine with the complexity of a propulsion system. Moreover, CubeSats are typically launched as a secondary payload together with a significantly larger and more expensive spacecraft. Due to launch safety considerations, storing propellant on the CubeSat would be a hazard for the main payload.

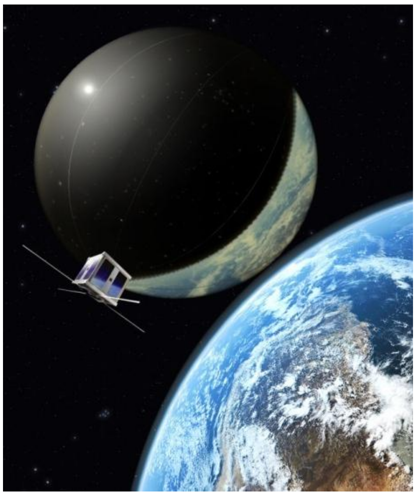

Figure 1: Artist's impression of a CubeSat with deployed reflective de-orbiting balloon (image credits: ESA, Aalborg University)

To enable higher altitude CubeSat missions a simple and reliable de-orbiting mechanism is needed that does not rely on aerodynamic drag or the use of propellant for orbit manoeuvres. Man-made orbital debris, consisting of obsolete spacecraft and disused launcher parts, is a growing concern for the future of space utilisation. In recent years, several guidelines have been published by governmental space agencies and international committees urging the disposal of spacecraft at the end-of-life to avoid the further accumulation of space debris [1]. The preferable method is de-orbiting of the satellite at the end of operations. An alternative is to transfer the spacecraft from its operational orbit into a so-called graveyard orbit. The latter option is less satisfactory because the dead satellite, due to external orbit perturbations, could potentially endanger operational satellites. However, a disposal orbit is the only viable option for high altitude spacecraft, when the Δv required for de-orbit is too high for conventional propulsion methods [2]. Alternative solutions have been identified which enhance aerodynamic and/or electrodynamic drag [3-6]. The former can be achieved by increasing the area-to-mass ratio (atm) of the spacecraft through the deployment of a large thin-film body. Electrodynamic drag uses the Earth's magnetic field to create a Lorentz force in opposite direction to the spacecraft's velocity by deploying a long, light-weight conductive tether which electrically charges in the ionosphere. Both methods are most effective close to the Earth, increasing the maximum initial orbit altitude from which de-orbit can be assured to 600–1000 km. Beyond this distance both perturbing effects become insignificant.

Previous work has proposed the use of solar radiation pressure for end-of-life manoeuvres by rotating the spacecraft's solar panels along the orbit to obtain a secular increase of the semi-major axis. This is achieved by orienting the solar panels to directly face the Sun when moving towards it and parallel to the incoming light when moving away from the Sun to decelerate the spacecraft [7]. This method, however, requires active pointing, thus placing high demands on the durability of the attitude control system and is thus not suitable for a low cost mission. In this paper a de-orbiting method is proposed which exploits the effect of solar radiation pressure (SRP) and Earth oblateness in combination with aerodynamic drag to passively de-orbit a satellite within a given time after the end-of-life without any further control requirements. This is achieved by making use of the interaction between SRP and J_2 effect to increase the eccentricity of any initially circular in-plane orbit until the perigee reaches an altitude at which the aerodynamic drag causes the spacecraft to de-orbit.

2. Orbital Dynamics

For an orbit which lies in the ecliptic plane and is only perturbed by solar radiation pressure (SRP) and the J_2 effect Krivov and Getino [8] found the expression of the Hamiltonian H which describes the e and ϕ phase space:

$$H = -\sqrt{1-e^2} + \alpha\, e \cos\phi - \frac{\kappa}{3\sqrt{1-e^2}^3} \tag{1}$$

where ϕ is the angle between the direction of the solar radiation and the direction of the orbit perigee from the centre of the Earth. Eq. (1) does not take into account solar eclipses and the tilt of the Earth's axis with respect to the ecliptic plane.

α is a parameter related to the influence of solar radiation pressure on the orbit and κ is related to the J_2 effect:

$$\alpha = \frac{3}{2\,n_{\odot}} a_{SRP} \sqrt{\frac{a}{\mu}} \tag{2}$$

$$\kappa = \frac{3}{2\,n_{\odot}} J_2 \, {R_E}^2 \sqrt{\frac{\mu}{a^7}} \tag{3}$$

where a_{SRP} is the acceleration the spacecraft experiences due to solar radiation pressure and can be calculated as:

$$a_{SRP} = c_R \frac{F_S}{c} \sigma \tag{4}$$

For a spherical spacecraft the area-to-mass ratio σ is not dependent on its attitude. While the parameter κ is only a function of the semi-major axis of the orbit, α is also dependent on the area-to-mass ratio and the coefficient of reflectivity of the spacecraft (c_R). A typical CubeSat has an atm of less than 0.01 m^2/kg. As such the effect of solar radiation pressure is almost insignificant for the orbit evolution. The inflation of a light-weight balloon, however, can change this dramatically. As can be seen in Figure 2, a 4 m diameter balloon can increase the area-to-mass ratio by a factor of 1000.

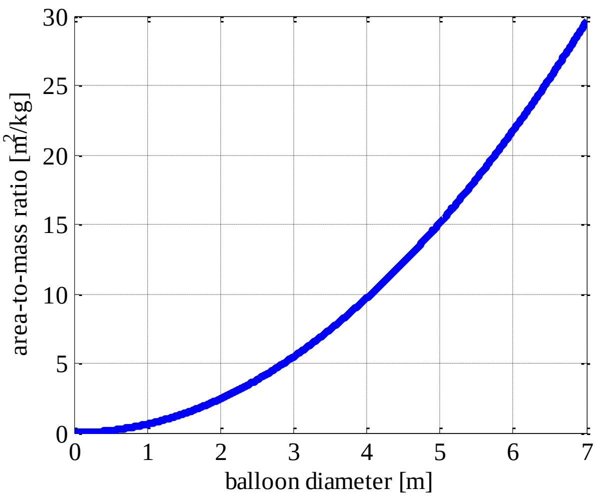

Figure 2: σ as a function of balloon diameter for a total spacecraft mass of 1.3 kg.

For increased area-to-mass ratios the orbital element phase space of e and ϕ exhibits interesting behaviour, particularly in the region of 2 - 3 R_E semi-major axis [8]. For a semi-major axis above approximately 12,350 km the phase space can display one of three behaviours depending on the area-to-mass ratio as shown in Figure 3. Above a certain σ threshold the maximum eccentricity e_{max} in the evolution of an initially circular orbit can be found at $\phi = 0$ (Figure 3c). At the critical area-to-mass ratio, σ_B, which is dependent on semi-major axis, the evolution of the initially circular orbit bifurcates and passes through a hyperbolic equilibrium at (e_B, π) (Figure 3b) to reach its maximum at ($e_{B,max}$, 0). Below this value of σ, the maximum eccentricity in the evolution of an initially circular orbit can be found at ($e_{1,max}$, π) (Figure 3a). In the last case, there also appears a second line corresponding to the same value of the Hamiltonian for the initially circular orbit that does not pass through e = 0 and has a minimum at ($e_{2,min}$, π) and a maximum at ($e_{2,max}$, 0). For semi-major axes below circa 12,350 km the behaviour always resembles that in Figure 3c. At semi-major axes larger than three Earth's radii the critical area-to-mass ratio, σ_B, and the bifurcation eccentricity, e_B, increase until they become irrelevant for this application and the behaviour can always be assumed to resemble Figure 3a.

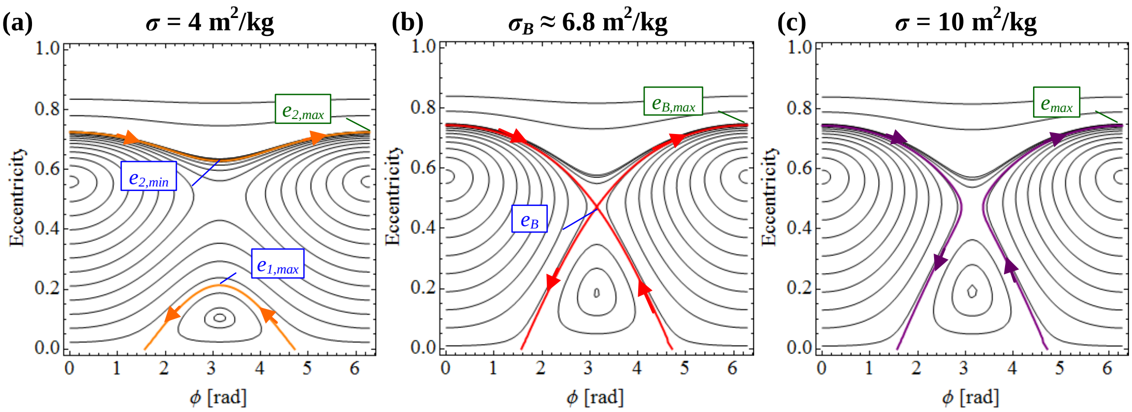

Figure 3: Phase plane diagram for a spacecraft with 15,000 km semi-major axis and a coefficient of reflectivity of c_R = 1.9 for three different values of σ. The bold coloured lines indicate the phase line for initial e = 0. The positions at which this phase line passes $\phi = \pi$ are marked in blue and the positions where it passes ϕ = 0 are marked in green.

An expression for the minimum required area-to-mass ratio to de-orbit spacecraft on initially circular orbits (e = 0) can be obtained by solving Eq. (1) which results in:

$$H_{circ} = -1 - \frac{\kappa}{3} \tag{5}$$

By inserting Eq. (5) into Eq. (1) and considering that the maximum eccentricity from a circular orbit can be reached at $\phi = \pi$ or $\phi = 0$ (see Figure 3), the resulting equation can be solved to give the required value of α needed to reach a certain eccentricity, e^*, from an initially circular orbit as a function of the semi-major axis:

$$\begin{aligned}\alpha_1(a,e^*) &= \frac{1-\sqrt{1-e^{*2}}}{e^*} + \left(\frac{1}{3e^*} - \frac{1}{3e^*\sqrt{1-e^{*2}}^3}\right)\kappa(a) \\ \alpha_2(a,e^*) &= -\left(\frac{1-\sqrt{1-e^{*2}}}{e^*} + \left(\frac{1}{3e^*} - \frac{1}{3e^*\sqrt{1-e^{*2}}^3}\right)\kappa(a)\right)\end{aligned} \tag{6}$$

The term α_1 corresponds to ϕ = 0 and α_2 to $\phi = \pi$, the two perigee angles for which the eccentricity can reach its maximum starting from e = 0. Since the semi-major axis is given by the spacecraft's circular operational orbit, the required area-to-mass ratio for any c_R can thus be calculated using Eqs. (2) and (4).

Figure 4(a) shows the solutions of Eq. (6) for a semi-major axis of 15,000 km. The noteworthy eccentricities highlighted in Figure 3 are marked in this diagram. The orange line indicates σ = 4 m²/kg and the purple line indicates σ = 10 m²/kg. The red line is where the phase line for initially circular orbits bifurcates with the critical area-to-mass ratio σ_B corresponding to α_B which is a function of semi-major axis. A problem arises when solving for an $e^* \in (e_B, e_{B,max})$. In this case Eq. (6) delivers lower values than α_B, but these correspond to the second identity phase line which never passes through e = 0. Thus, to reach values of eccentricity between the hyperbolic equilibrium point (e_B in Figure 3b) and the maximum eccentricity reachable through the bifurcated zero-eccentricity phase line ($e_{B,\max}$ in Figure 3b), the minimum area-to-mass ratio solution corresponds to the bifurcated phase plane. Figure 4b shows the revised function for the required area-to-mass ratio to reach e^* at a = 15,000 km. It is the result of the following decision tree:

$$\begin{array}{ll} \text{for } e^* < e_B & \rightarrow \alpha = \alpha_2(a, e^*) \\ \text{for } e_B \leq e^* \leq e_{B,max} & \rightarrow \alpha = \alpha_B(a) \\ \text{for } e^* > e_{B,max} & \rightarrow \alpha = \alpha_1(a, e^*) \end{array} \tag{7}$$

α_B is found through the bifurcating eccentricity $e_B(a)$ which is determined by locating the local extremum in (6) with $e_B \in [0,1]$:

$$\frac{\partial \alpha_{1,2}(a, e_B(a))}{\partial e_B(a)} = 0 \tag{8}$$

$$\alpha_B(a) = \alpha_2(a, e_B(a)) \tag{9}$$

The eccentricity needed to de-orbit a spacecraft is called critical eccentricity, e_{crit} and is a function of the semi-major axis and the required perigee altitude, h, to be reached,

$$e_{crit} = 1 - \frac{R_E + h}{a} \tag{10}$$

We continue to work with h = 0 km as a worst case assumption, neglecting the effect of drag that, below approximately 600 km altitude, will facilitate the final decay [9]. Both κ and e_{crit} are solely dependent on the initial orbit's semi-major axis. We can therefore determine the minimum area-to-mass ratio required for de-orbit as a function of a by substituting $e^* = e_{crit}$ into Eq. (6). Note, however, that this result does not take into any consideration of the transfer time for de-orbit. It has already been established that at some semi-major axes the spacecraft orbit would move on a phase plane line which passes through a hyperbolic equilibrium point where it would slow down asymptotically (see Figure 3b). In this case the time covered for transferring the spacecraft from e = 0 to the desired e_{crit} tends to infinity.

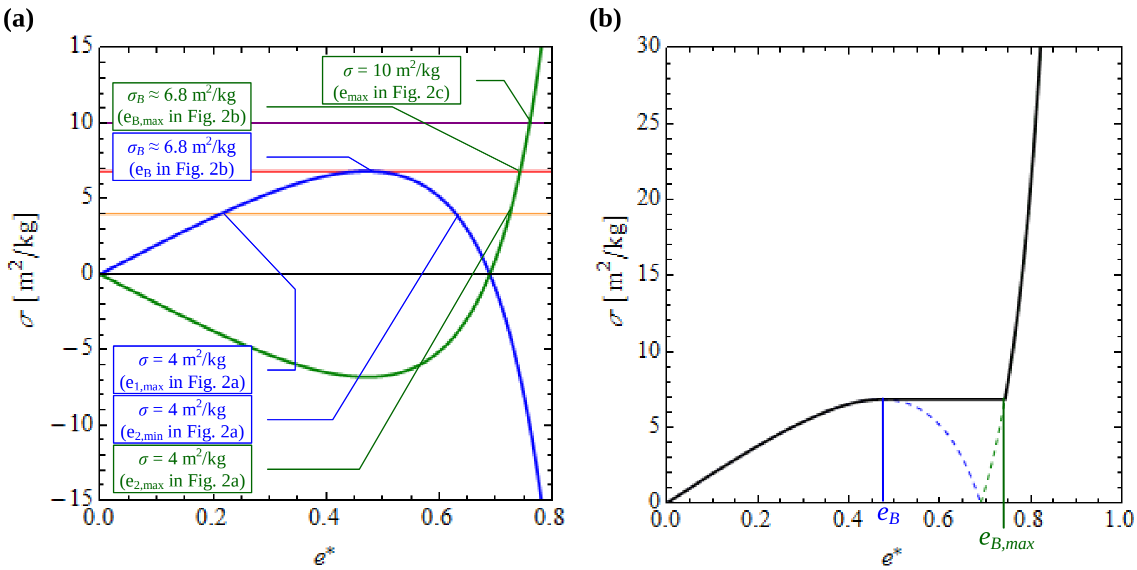

Figure 4: (a) Area-to-mass ratio computed through Eq. (6) with c_R = 1.9 for a semi-major axis of 15,000 km. The blue line represents the case in which the maximum eccentricity can be reached at $\phi = \pi$, the green line the case in which the maximum eccentricity can be reached at ϕ = 0. (b) Minimum area-to-mass ratio required to reach eccentricity e^* for a semi-major axis of 15,000 km taking the double identity of the phase line into account (black line). The dashed lines represent the solutions of Eq. (6).

To find the actual minimum area-to-mass ratio a numerical solution has to be found for a maximum de-orbiting time. Figure 5 shows the required area-to-mass ratio for three different maximum de-orbiting times, along with the analytical solution (black line). It can be seen that a minimum in required area-to-mass ratio exists for a semi-major axis of about 13,500 km. The lowest value increases significantly for shorter de-orbiting times. However, since the device operates completely passively after deployment a longer decay time is not a risk to the success of the de-orbiting manoeuvre.

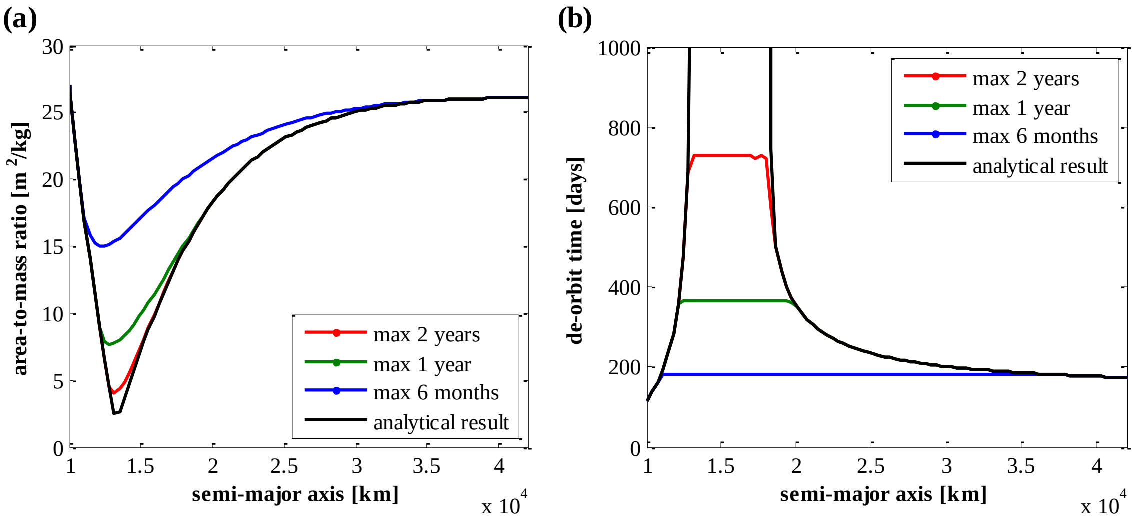

Figure 5: Analytical results (black) compared to numerical results with different maximum de-orbiting times. (a) Minimum area-to-mass ratio required for de-orbiting and (b) time until de-orbiting as a function of semi-major axis.

3. System Design

In this section one possible design for a de-orbiting subsystem is described. The aim is to have a reflective balloon which minimises stored volume and mass and can be reliably deployed at the end of the mission until the spacecraft can be successfully de-orbited. For this three main factors are important: the light-weight reflective balloon material, the deployment mechanism, and the rigidisation material and method. The key drivers are reliability, cost and space and mass efficiency.

The material chosen for the balloon membrane is a 10 μm silvered aluminium-oxide coated Kapton film, which has been impregnated with a rigidising resin. Kapton has been successfully used in space applications and offers good reliability [10]. Although thinner Kapton films have been developed, the 10 μm thickness was chosen as a trade-off between the main design drivers of reliability and mass efficiency. Kapton polyamide films have a density of 1420 kg/m^3. Possible options for deployment include mechanical methods and gas-based inflation, where the gas can be stored in compressed form or be generated in a cold gas generator. A nitrogen gas generator is selected for inflation of the balloon. This mechanism satisfies the key drivers since it can be manufactured cheaply, is very reliable and mass and volume efficient. For 0.5 g of nitrogen one micro gas generator is required which measures 15 cm^3 and weighs of order 8 g [11]. An inflation pressure of 10^{-4} bar is assumed which leads to one generator per 4.35 m^3 of balloon volume using the ideal gas equation and assuming the nitrogen is at room temperature at inflation. For smaller volumes the balloon can be inflated as a whole. For larger devices the inflation of veins along the surface is suggested.

The rigidisation of the balloon after deployment is achieved by impregnating the skin with a resin which hardens at low temperatures. While the balloon is inside the spacecraft it is assumed to be at standard operating temperature (room temperature). After release it quickly looses heat due to the optical properties of the material. It is highly reflective with an absorptivity of only 0.08 and an emissivity of 0.19 [12]. An ESATAN finite element analysis of the thermal worst case with a constant attitude towards the sun shows the maximum equilibrium surface temperature to be less than -20° C (see Figure 6). The thermal capacity and conductivity of the balloon are very low because of its thin surface. However, the temperature of the sun-facing side is kept close to that of the shadow side by covering the inside of the balloon skin with a black carbon layer which is highly emissive and guarantees a good heat exchange between the sun exposed side and the shadow side of the device.

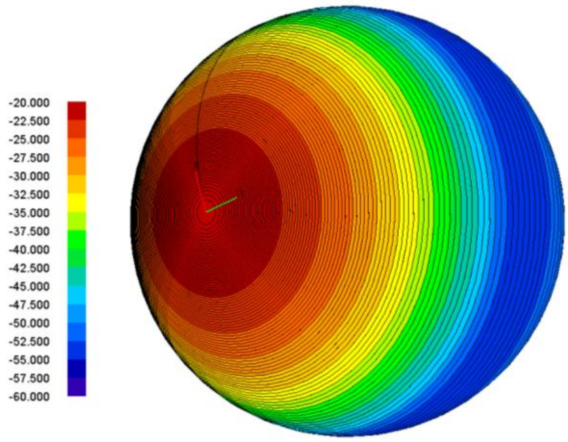

Figure 6: ESATAN temperature results of a worst case steady state analysis.

Figure 7a shows the volume and mass ratio of the stowed de-orbiting subsystem in relation to a 1.3 kg CubeSat calculated using the design parameters described in this section. Figure 7b shows the mass ratio for this device compared to the mass of propellant needed to perform a single impulse manoeuvre to lower the perigee enough to de-orbit.

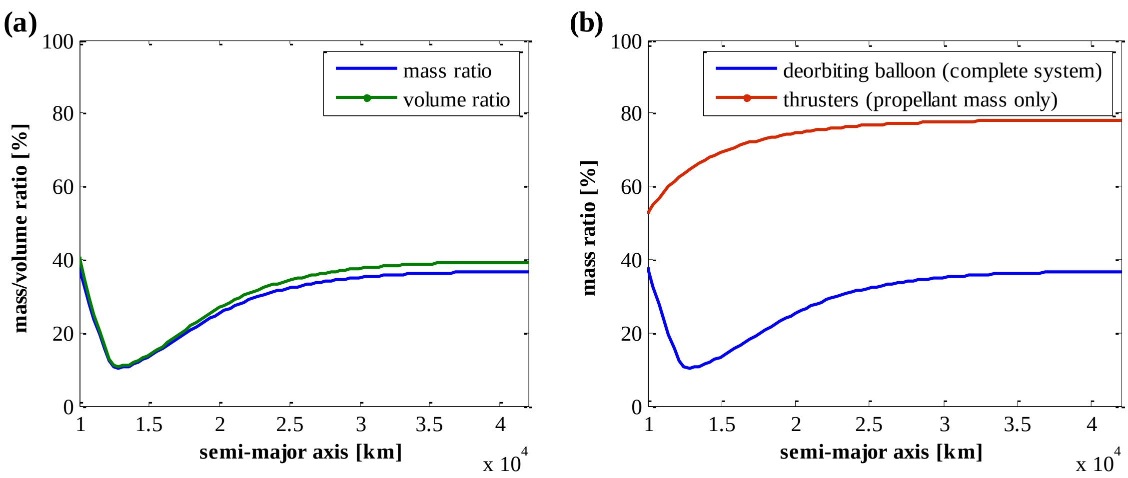

Figure 7: (a) Required volume and mass ratios of the stowed de-orbiting balloon in a CubeSat system for a maximum de-orbiting period of 365 days and (b) comparison with mass ratio of propellant only for single impulse manoeuvre for a thruster system with I_{sp} = 320s.

4. Conclusions

A de-orbiting balloon has been shown to be a feasible solution for the de-orbiting of small satellites in circular low inclination orbits. It is significantly more mass efficient than propulsion-based solutions even at very high altitudes such as geostationary orbits. It is most efficient, however, for altitudes of 1 to 1.5 Earth radii. The use of solar radiation pressure to increase the orbit eccentricity enables passive de-orbiting from significantly higher altitudes than conventional drag augmentation devices without any additional risk to the main payload at launch. Additionally this method provides a significant advantage over comparable low-thrust solutions because the de-orbiting manoeuvre will take place completely passively after the deployment of the balloon. Thus, any damage to the flight systems sustained from traversing the radiation belts cannot affect the reliability of the method.

Future work will extend the model to consider the tilt of the Earth axis and to include atmospheric drag in a 3D numerical orbit propagation. The latter will likely improve the results as a lower eccentricity will be needed to de-orbit.

References

[1] IADC, IADC Space Debris Mitigation Guidelines. Inter-Agency Space Debris Coordination Committee (2002)

[2] Burkhardt, H., *et al.*, Evaluation of Propulsion Systems for Satellites End-of-Life De-orbiting. 38th AIAA/ASME/SAE/ASEE Joint Propulsion Conference & Exhibit (2002)

[3] Roberts, P. C. E., and Harkness, P. G., Drag Sail for End-of-Life Disposal from Low Earth Orbit. *Journal of Spacecraft and Rockets* 44, 6, 9 (2007)

[4] Maessen, D. C., *et al.*, Development of a Generic Inflatable De-orbit Device for CubeSats. International Astronautical Congress (2007)

[5] Iess, L., *et al.*, Satellite de-orbiting by means of electrodynamic tethers part I: General concepts and requirements. *Acta Astronautica* 50, Compendex, 399-406 (2002)

[6] Hoyt, R. P., *et al.*, The Terminator Tape: A cost-effective de-orbit module for end-of-life disposal of LEO satellites. AIAA Space 2009 Conference and Exposition, September 14, 2009 - September 17, 2009 (2009)

[7] Borja, J. A., and Tun, D., Deorbit process using solar radiation force. *Journal of Spacecraft and Rockets* 43, 685-687 (2006)

[8] Krivov, A. V., and Getino, J., Orbital evolution of high-altitude balloon satellites. *Astronomy and Astrophysics* 318, 308-314 (1997)

[9] Colombo, C., and McInnes, C. R., Orbital dynamics of Earth-orbiting ‘smart dust’ spacecraft under the effects of solar radiation pressure and aerodynamic drag. AIAA Guidance, Navigation, and Control Conference (2010)

[10] Freeland, R. E., *et al.*, Inflatable Deployable Space Structures Technology Summary. 49th International Astronautical Congress (1998)

[11] Van Der List, M. C. A. M., *et al.*, Applications for solid propellant cool gas generator technology. 4th International Spacecraft Propulsion Conference (2004)

[12] Gilmore, D. G. *Spacecraft Thermal Control Handbook, Volume 1*. American Institute of Aeronautics and Astronautics/Aerospace Press. (2002)